



Inflammation differentially controls transport of depolarizing Nav versus hyperpolarizing Kv channels to drive rat nociceptor activity

Grant P. Higerd-Rusli^{a,b,c,d,e} , Sidharth Tyagi^{a,b,c,d,f}, Christopher A. Baker^{b,c,d} , Shujun Liu^{b,c,d}, Fadia B. Dib-Hajj^{b,c,d}, Sulayman D. Dib-Hajj^{b,c,d,1} , and Stephen G. Waxman^{b,c,d,1}

Edited by Nieng Yan, Princeton University, Princeton, NJ; received September 8, 2022; accepted December 28, 2022

Inflammation causes pain by shifting the balance of ionic currents in nociceptors toward depolarization, leading to hyperexcitability. The ensemble of ion channels within the plasma membrane is regulated by processes including biogenesis, transport, and degradation. Thus, alterations in ion channel trafficking may influence excitability. Sodium channel $\text{Na}_v1.7$ and potassium channel $\text{K}_v7.2$ promote and oppose excitability in nociceptors, respectively. We used live-cell imaging to investigate mechanisms by which inflammatory mediators (IM) modulate the abundance of these channels at axonal surfaces through transcription, vesicular loading, axonal transport, exocytosis, and endocytosis. Inflammatory mediators induced a $\text{Na}_v1.7$ -dependent increase in activity in distal axons. Further, inflammation increased the abundance of $\text{Na}_v1.7$, but not of $\text{K}_v7.2$, at axonal surfaces by selectively increasing channel loading into anterograde transport vesicles and insertion at the membrane, without affecting retrograde transport. These results uncover a cell biological mechanism for inflammatory pain and suggest $\text{Na}_v1.7$ trafficking as a potential therapeutic target.

pain | inflammation | ion channels | intracellular trafficking | neuronal excitability

Pain provides powerful motivation to alter behavior and promote healing. The dorsal root ganglia (DRG) and trigeminal ganglia contain pain-sensing neurons—nociceptors—which relay information regarding tissue damage to the central nervous system (1, 2). Hyperactivity in peripheral sensory neurons is an obligate component of most pain (3). Neuronal excitability is determined by the balance of depolarizing and hyperpolarizing currents produced by ion channels at the cell surface (4). In these and other neurons, currents produced by voltage-gated sodium (Na_v) channels and voltage-gated potassium (K_v) channels underlie the depolarizing and hyperpolarizing phases of the action potential, respectively (5).

The balance of ionic currents at the neuronal surface, and thus neuronal excitability, is a function of the number and physiological properties of specific channels inserted at the membrane. Therefore, various processes of channel biogenesis and trafficking—including transcription, translation, transport, exocytosis, endocytosis, recycling, and degradation—are key determinants of neuronal activity and the resulting sensory experience (6). This is especially relevant in peripheral sensory axons, in which signals are initiated distally and propagated over vast distances, sometimes exceeding a meter. Thus, the trafficking of ion channels could potentially be targeted to modulate neuronal activity. However, whether regulation of ion channel trafficking to distal ends of axons plays a causal role in pain and whether mechanisms for regulation of trafficking of specific channel types exist is unclear.

While multiple Na_v isoforms are expressed in peripheral sensory neurons, $\text{Na}_v1.7$ plays critical roles in setting the firing threshold of these cells and releasing neurotransmitter in the spinal cord dorsal horn (7). Further, genetic studies have identified $\text{Na}_v1.7$ as an obligate, bidirectional modulator of pain in humans – gain-of-function mutations in $\text{Na}_v1.7$ cause extreme pain syndromes, while its loss-of-function can cause complete insensitivity to painful stimuli (8). In contrast, potassium channels underlying the M-current— $\text{K}_v7.2/3$ —have been identified as inhibitors of DRG activity and promoters of pain resilience (9, 10). Further, these classes of channels have been shown to be pathologically regulated in manners consistent with their physiological roles; expression of $\text{Na}_v1.7$ is up-regulated, while $\text{K}_v7.2$ is down-regulated in models of inflammatory pain and neuropathy (11–17). Finally, both $\text{Na}_v1.7$ and K_v7 channels are localized in the distal axons of peripheral sensory neurons (18, 19). These factors, as well as the preferential expression of $\text{Na}_v1.7$ in peripheral neurons, have motivated efforts to pharmacologically target the conductance of channels present at the cell membrane (20, 21).

We previously demonstrated that $\text{Na}_v1.7$ currents, anterograde channel trafficking, and abundance at the surface of distal axons are up-regulated in models of inflammation

Significance

The burden of pain is immense, and current treatments are often ineffective and addictive. Activity in pain-sensing neurons is promoted by proexcitatory (Na_v) channels and inhibited by antiexcitatory voltage-gated potassium (K_v) channels. $\text{Na}_v1.7$ is a promising target for nonaddictive pain treatment, and modulating its transport to axonal membranes is a potential therapeutic strategy. However, this approach requires identifying mechanisms which differentially regulate trafficking of $\text{Na}_v1.7$ channels over other channels such as $\text{K}_v7.2$. We investigated channel trafficking in live neurons and found that inflammatory mediators (IM) increase $\text{Na}_v1.7$ surface density through vesicular loading and axonal transport, without similarly increasing $\text{K}_v7.2$ transport. Thus, trafficking of $\text{Na}_v1.7$ is differentially regulated by inflammation to promote pain and might be targeted therapeutically.

Author contributions: G.P.H.-R., S.D.D.-H., and S.G.W. designed research; G.P.H.-R. and S.T. performed research; S.L. and F.B.D.-H. contributed new reagents/analytic tools; G.P.H.-R., S.T., and C.A.B. analyzed data; and G.P.H.-R., S.T., S.D.D.-H., and S.G.W. wrote the paper.

The authors declare no competing interest.

This article is a PNAS Direct Submission.

Copyright © 2023 the Author(s). Published by PNAS. This article is distributed under Creative Commons Attribution-NonCommercial-NoDerivatives License 4.0 (CC BY-NC-ND).

¹To whom correspondence may be addressed. Email: sulayman.dib-hajj@yale.edu or stephen.waxman@yale.edu.

This article contains supporting information online at <https://www.pnas.org/lookup/suppl/doi:10.1073/pnas.2215417120/-DCSupplemental>.

Published March 10, 2023.

and chemotherapy-induced peripheral neuropathy (22, 23). However, we have also shown that $\text{Na}_V1.7$ and multiple other ion channels, including $\text{K}_V7.2$, are trafficked to axons together in the same vesicles (24). Thus, it is unclear whether the upregulation of $\text{Na}_V1.7$ channel trafficking in response to inflammation represents a specific effect on $\text{Na}_V1.7$ or a nonspecific increase in axonal trafficking of multiple proteins. Further, the specific cell biological mechanisms which mediate this effect are also unknown.

Here, we demonstrate that inflammatory mediators (IM) induce an increase in spontaneous activity in distal axons, which is dependent on $\text{Na}_V1.7$ channels. We also developed multiple imaging assays utilizing microfluidic chambers (MFCs) and self-labeling protein tags to investigate multiple distinct trafficking processes including vesicular loading, anterograde and retrograde trafficking, exocytosis, and endocytosis of ion channels in real time. We show that treatment of sensory neurons with IM specifically up-regulates the abundance of $\text{Na}_V1.7$ at the surface of distal axons by increasing its vesicular loading, anterograde trafficking, and membrane insertion, without a corresponding increase in channel removal. However, IM treatment did not have similar effects on $\text{K}_V7.2$. Together, these findings suggest a causal role for the regulation of $\text{Na}_V1.7$ trafficking in inflammatory pain and point to vesicular loading of $\text{Na}_V1.7$ as a potential therapeutic target.

Results

Inflammatory Mediators Induce an $\text{Na}_V1.7$ -Dependent Increase in Axonal Activity. First, we sought to determine whether the IM cocktail causes an increase in activity in distal axons, and whether that activity is dependent on $\text{Na}_V1.7$ channels. To do this, we transfected DRG neurons with Axon-jGCaMP8m, a genetically encoded calcium indicator which is trafficked to axons, and cultured them in MFCs (microfluidic chambers) (25). We then treated the neurons (both the axon and soma chambers) with IM for 4 h and washed it away before acquiring time-lapse images of calcium activity in distal axons. Since we imaged the axons after washing the IM treatment away, the activity we observed can be understood as spontaneous activity influenced by a prior stimulus rather than directly stimulus evoked. After acquiring an initial set of baseline movies, we added the selective $\text{Na}_V1.7$ blocker ProTx-II (26) to determine whether $\text{Na}_V1.7$ channels are necessary for the observed activity (Fig. 1 A and B). Axons treated with IM exhibited a significantly higher rate of calcium events compared to untreated axons (Fig. 1 C–E). Further, ProTx-II treatment normalized the frequency of calcium events in IM-treated axons (Fig. 1 D and E). ProTx-II treatment also reduced, but did not eliminate, calcium events in control neurons (Fig. 1 C and E). This demonstrates that IM treatment induces an increase in axonal activity and that $\text{Na}_V1.7$ channels are necessary for this heightened activity.

Inflammatory Mediators Increase $\text{Na}_V1.7$ Current, but Not M-Current. We previously demonstrated that IM treatment results in an increase in $\text{Na}_V1.7$ current in DRG neurons (22). First, we confirmed this effect using voltage-clamp recordings from $\text{Na}_V1.8$ -null DRG neurons expressing h $\text{Na}_V1.7\text{R}$ channels. In cells treated with IM, mean peak $\text{Na}_V1.7$ current roughly doubled from -28.8 nA to -56.3 nA and current density increased similarly from -1.22 nA/pF to -2.57 nA/pF (Fig. 2 A and B), which is similar to our previous observation (22).

Next, we sought to determine whether IM treatment also affects the endogenous M-current—a hyperpolarizing potassium current mediated by heterotetrameric $\text{K}_V7.2/3$ channels, which antagonizes

activity in DRG neurons and other neurons (27). Using a previously described protocol (*Methods*) to evoke the M-current, we observed a trend toward a decrease in M-current and current density in DRG neurons treated with IM relative to control condition, though these differences did not reach statistical significance (Fig. 2 C and D) ($P = 0.14$ and 0.10 , respectively). Note that the axis in (Fig. 2B) is negative while that in (Fig. 2D) is positive, because $\text{Na}_V1.7$ and M-currents are inward (negative) and outward (positive), respectively. Together, these results confirm that IM up-regulates $\text{Na}_V1.7$ current without altering the M-current and demonstrates a trend toward opposite regulation of these channels with opposing physiological functions.

Inflammatory Mediators Increase the Abundance of $\text{Na}_V1.7$, but Not $\text{K}_V7.2$ at the Surface of Axons. Since the amount of $\text{Na}_V1.7$ present at the surface of distal axons increases in response to IM (22), we next investigated whether this effect is specific to $\text{Na}_V1.7$ or extends to the functionally opposing channel $\text{K}_V7.2$. We transfected rat DRG neurons with Halo- $\text{Na}_V1.7$ or $\text{K}_V7.2$ -Halo and cultured them in MFCs for 5 to 6 d. Halo-tag is a self-labeling enzymatic tag which reacts covalently with a specific cognate ligand which can be conjugated to a variety of synthetic fluorophores. Four hours prior to imaging, the neurons (both axons and somas) were treated with an IM cocktail or vehicle. $\text{Na}_V1.7$ or $\text{K}_V7.2$ channels at the surface of axons were then labeled using cell-impermeable JF635i-Halo-tag Ligand (Fig. 2E).

Fluorescence intensity of surface-labeled $\text{Na}_V1.7$ channels was approximately twofold higher in axons which had been treated with IM compared to vehicle-treated axons, confirming the effect we showed previously (Fig. 2 F and H) (22). In contrast, the fluorescence intensity of $\text{K}_V7.2$ channels at the surface of distal axons was not affected by IM treatment (Fig. 2 G and H). This suggests that the IM-induced upregulation of $\text{Na}_V1.7$ surface expression in axons is specific, and not part of a general upregulation of ion channel trafficking.

Inflammatory Mediators Do Not Modulate $\text{Na}_V1.7$ or $\text{K}_V7.2$ Transcription on the Timescale of Hours. To test whether the IM-induced changes in channel surface expression and current could be caused by changes in expression of the endogenous channel genes on this relatively short timescale, we performed RT-qPCR. DRG neurons were cultured and treated with IM cocktail for either 4 or 24 h before messenger ribonucleic acid (mRNA) was isolated and quantified. Neither $\text{Na}_V1.7$ nor $\text{K}_V7.2$ mRNA expression was significantly changed by either duration of IM treatment compared to control (*SI Appendix*, Fig. S1). This confirms that the increase in $\text{Na}_V1.7$ surface expression in distal axons after 4 h of IM exposure occurs without an increase in expression at the transcriptional level.

Inflammatory Mediators Do Not Alter $\text{Na}_V1.7$ or $\text{K}_V7.2$ Endosome Dynamics. Since the anterograde trafficking of $\text{Na}_V1.7$ to distal axons increases in response to IM (22), we investigated the effect of this treatment on the retrograde trafficking of $\text{Na}_V1.7$ -containing and $\text{K}_V7.2$ -containing endosomes. Following the protocol in Fig. 2E, $\text{Na}_V1.7$ channels at the surface of axons were labeled and then imaged over the course of an hour. Fluorescently labeled channels are initially limited to the cell surface but over time are internalized and transported retrogradely in endosomes (*SI Appendix*, Fig. S2A). Kymographs of these axons were generated to quantify endosome intensity, flux, and velocity (*SI Appendix*, Fig. S2 B and C). A kymograph is a transformation of time-lapse movie data into a two-dimensional image, plotting distance along the axon on the x axis and elapsed time on the y axis.

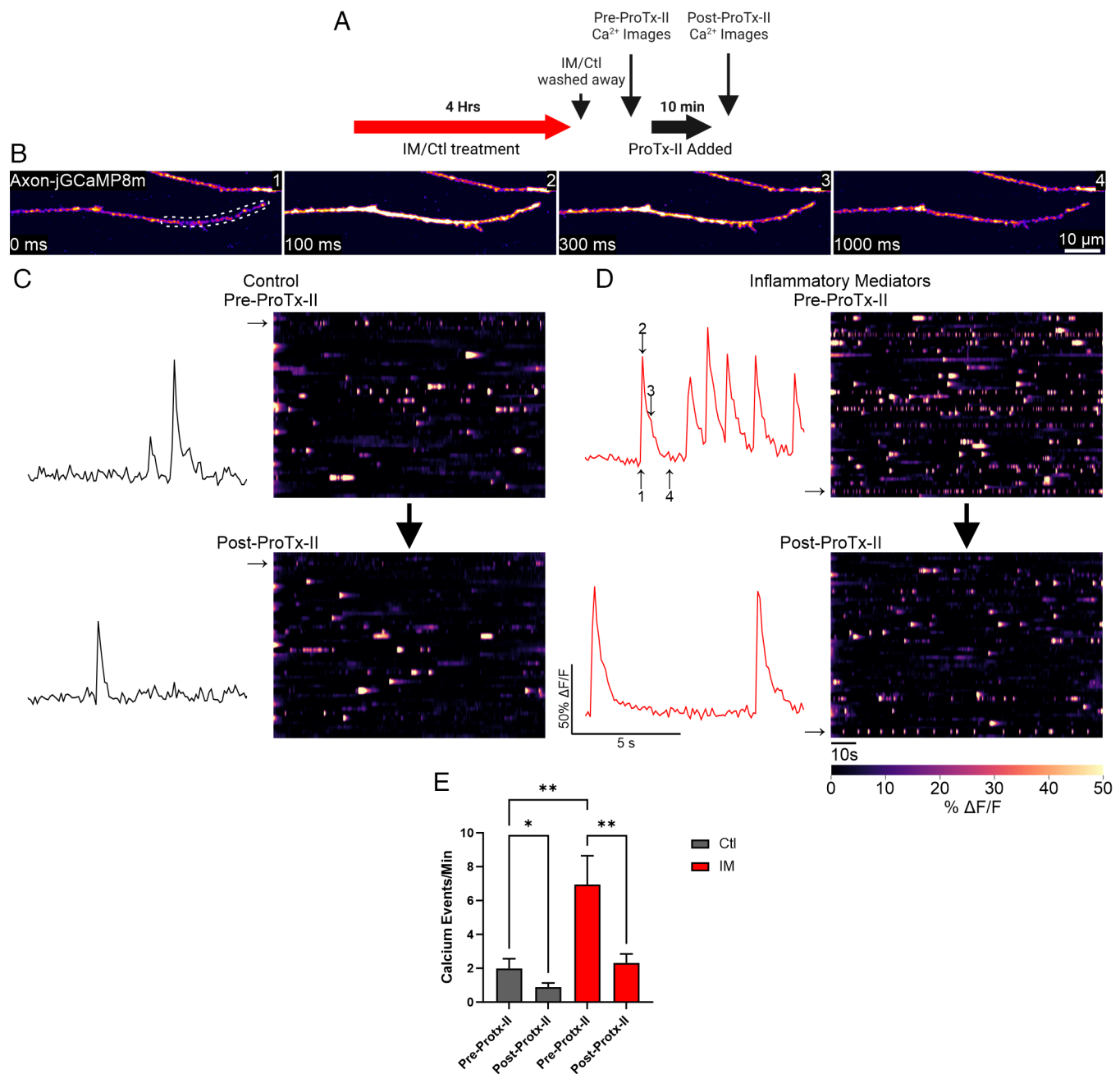


Fig. 1. Inflammatory mediators induce an increase in axonal excitability which is dependent on $\text{Na}_\text{v}1.7$. (A) DRG neurons were transfected with Axon-jGCaMP8m and cultured in MFCs for 5 to 6 d. Both the axon and soma compartments were treated with IM cocktail or normal media for 4 h. Then, the treatment was removed by thoroughly washing both chambers with DRG NIS. Multiple fields of view containing GCaMP-expressing axonal ends were selected and green time-lapse movies were acquired. Then, DRG NIS containing 10 nM ProTx-II (a selective $\text{Na}_\text{v}1.7$ blocker) was added to both chambers by fluid exchange and the same axons were imaged again. (B) Still images of a time-lapse movie show changing GCaMP fluorescence over time in a distal axon end. Intensity measurements were taken from the distal-most 30 μm of the axon (indicated by the dotted white line, left image). (C and D) Left: Spikes in GCaMP fluorescence indicate axonal activity. The vertical arrows labeled 1 to 4 in (D) correspond to the timepoints of the images in (B). Right: Raster plots display the time-course GCaMP signal of one axon per row. The rows which correspond to the traces to the left are indicated with horizontal arrows. (E) The frequency of calcium events was ~3.5-fold higher in IM-treated axons compared to control axons ($P = 0.002$, Mann-Whitney test with Bonferroni correction). Addition of ProTx-II to block $\text{Na}_\text{v}1.7$ current decreased the activity in IM-treated axons by 66% and in control axons by 45% ($P = 0.002$ and 0.043, respectively, Wilcoxon paired tests with Bonferroni correction, three independent cultures, $N = 41$ to 45 axons).

$\text{Na}_\text{v}1.7$ -containing endosomes and $\text{K}_\text{v}7.2$ -containing endosomes in IM-treated axons had similar intensity, flux, and velocity as those in control axons (SI Appendix, Fig S2 D and E). Together, these results show that inflammatory mediators do not modulate endocytic trafficking of $\text{Na}_\text{v}1.7$ or $\text{K}_\text{v}7.2$.

Inflammatory Mediators Increase $\text{Na}_\text{v}1.7$ Trafficking in the Anterograde Direction More Than $\text{K}_\text{v}7.2$, and Do Not Regulate Retrograde Trafficking of Either. We next developed an assay

to directly compare the flow of ion channels in anterograde and retrograde directions within individual axons. DRG neurons were transfected with Halo-tagged channels and cultured in MFCs. The IM cocktail was then added to both soma and axon chambers for 4 h prior to imaging. JF549-Halo-tag Ligand was added to the soma chamber and JF646-Halo-tag Ligand was added to the axon chamber. Vesicles undergoing trafficking through the microgroove barriers which separate the two chambers were imaged separately using red and far-red imaging (Fig. 3A). $\text{Na}_\text{v}1.7$ trafficking in

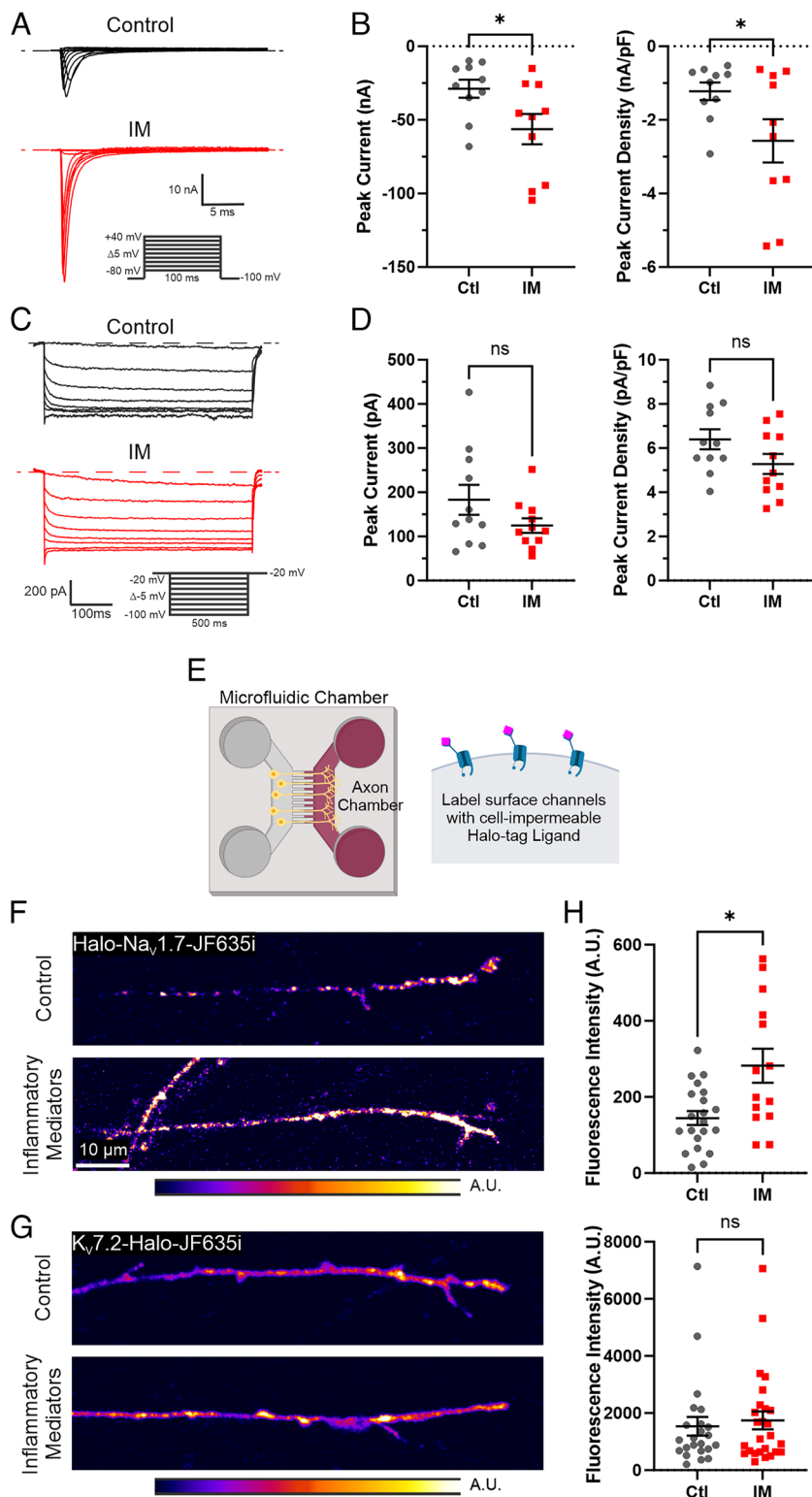


Fig. 2. Inflammatory mediators increase $\text{Na}_V1.7$ current and surface expression, but not M-current or $\text{K}_V7.2$ surface expression. (A) Representative current traces from $\text{Na}_V1.8$ -null DRG neurons expressing $\text{Na}_V1.7$ channels in control and IM-treated conditions. $\text{Na}_V1.7$ current traces were evoked by 100-ms depolarizing voltage steps from -80 mV to $+40 \text{ mV}$ in 5 mV increments from a holding potential of -100 mV . (B) IM treatment increased peak inward current (Left) and current density (Right) compared to control neurons ($n = 10$ each, $P < 0.05$). Peak current density was defined by normalizing the maximal current evoked from the voltage protocol to the cellular capacitance. (C) M-current families were evoked by a series of 500-ms hyperpolarizing voltage steps from -20 mV to -100 mV in 5 mV increments from a holding potential of -20 mV . Representative M-current traces from rat DRG neurons in control and IM-treated conditions. M-current was assessed as the difference in instantaneous peak current at the beginning of the command step and the steady-state current just before command offset. (D) IM treatment led to a trend toward decreased peak M-current (Left) and current density (Right), which did not reach statistical significance ($n = 11$ each, $P = 0.14$ and 0.10, respectively). Note that the axis in (Fig. 2B) is negative while that in (Fig. 2D) is positive, because $\text{Na}_V1.7$ and M-currents are inward (negative) and outward (positive), respectively. (E) DRG neurons were transfected with $\text{Halo-Na}_V1.7$ or $\text{K}_V7.2$ -Halo and cultured in MFCs for 5 d. Both soma and axon chambers were then treated for 4 h with either an inflammatory mediator cocktail (IM) or normal media (Ctl). Channels at the axonal surface were then labeled with cell-impermeable JF635i-Halo-tag ligand. (F and G) Fluorescence images of IM-treated vs control axon endings. (H) Mean fluorescence of $\text{Na}_V1.7$ at the surface of distal axons was twofold higher in IM-treated axons compared to Ctl axons ($N = 14$ to 21 axons, $P = 0.01$). Mean fluorescence of $\text{K}_V7.2$ at the axonal surface was similar in IM-treated and Ctl axons ($N = 23$ to 26 axons, $P = 0.71$). Unpaired t tests. Error bars represent mean \pm SEM.

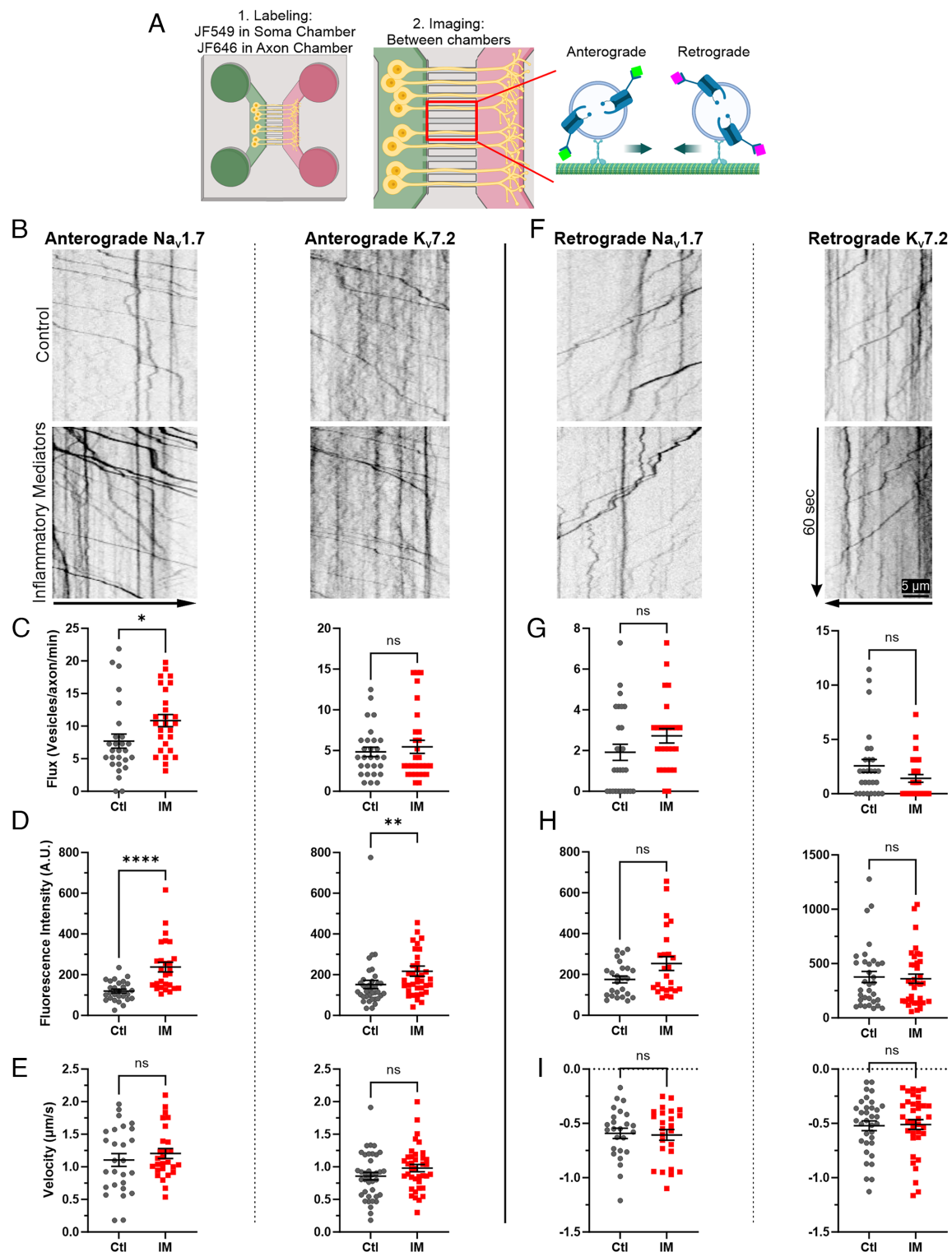


Fig. 3. Inflammatory mediators increase anterograde trafficking of $\text{Na}_v1.7$ more than $\text{K}_v7.2$, but do not regulate retrograde trafficking of either. (A) DRG neurons were transfected with Halo- $\text{Na}_v1.7$ or $\text{K}_v7.2$ -Halo and cultured in MFCs for 5 d. Both soma and axon chambers were then treated for 4 h with either an inflammatory mediator cocktail (IM) or normal media (Ctl). Channels in the soma compartment were labeled with cell-permeable, red JF549-Halo-tag ligand, while channels in the axonal compartment were labeled with cell-permeable, far-red JF646-Halo-tag ligand. After labeling, anterograde vesicles were visualized using red imaging and separately, retrograde vesicles were visualized using far-red imaging as they were transported between the two chambers. (B) Kymographs show vesicles containing $\text{Na}_v1.7$ or $\text{K}_v7.2$ (*Left* and *Right*, respectively) moving in the anterograde direction. (C) Anterograde flux (# of vesicles/axon/min) of vesicles carrying $\text{Na}_v1.7$ was 67% higher in axons treated with IM relative to control axons in the anterograde direction (*Left*, $N = 27$ axons each, $P = 0.01$), but was similar for vesicles carrying $\text{K}_v7.2$ (*Right*, $N = 28$ to 29 axons each, $P = 0.95$). (D) Fluorescence intensity of $\text{Na}_v1.7$ in anterograde vesicles was twofold greater in axons treated with IM (*Left*, $N = 27$ axons each, $P < 0.0001$), and intensity of $\text{K}_v7.2$ in anterograde vesicles was 45% greater in axons treated with IM (*Right*, $N = 37$ axons each, $P = 0.004$). (E) Velocity of anterograde $\text{Na}_v1.7$ vesicles and $\text{K}_v7.2$ vesicles was similar in axons treated with IM compared to control axons ($\text{Na}_v1.7$: *Left*, $N = 27$ axons each, $P = 0.43$. $\text{K}_v7.2$: *Right*, $N = 38$ axons each, $P = 0.13$). (F) Kymographs show vesicles containing $\text{Na}_v1.7$ or $\text{K}_v7.2$ moving in the retrograde direction. (G) Retrograde flux of vesicles containing $\text{Na}_v1.7$ or $\text{K}_v7.2$ was similar in IM and control axons ($\text{Na}_v1.7$: *Left*, $N = 26$ to 27 axons each, $P = 0.07$. $\text{K}_v7.2$: *Right*, $N = 28$ axons each, $P = 0.12$). (H) Intensity of $\text{Na}_v1.7$ and $\text{K}_v7.2$ fluorescence in retrograde vesicles was not significantly different in IM-treated axons ($\text{Na}_v1.7$: *Left*, $N = 25$ axons each, $P = 0.10$. $\text{K}_v7.2$: *Right*, $N = 33$ to 36 axons each, $P = 0.96$). (I) Velocity of $\text{Na}_v1.7$ - or $\text{K}_v7.2$ -containing retrograde vesicles was similar in IM-treated and control axons ($\text{Na}_v1.7$: *Left*, $N = 25$ axons each, $P = 0.83$. $\text{K}_v7.2$: *Right*, $N = 34$ to 36 axons each, $P = 0.86$).

the anterograde direction was up-regulated in response to IM (Fig. 3 *B*, *Left*), with a 67% increase in vesicular flux and 100% increase in fluorescence intensity per vesicle (Fig. 3 *C* and *D*, *Left*), but there was no difference in vesicle velocity (Fig. 3 *E*, *Left*). The same experiment was performed with K_V7.2-Halo (Fig. 3 *B*, *Right*). While there was no difference in flux or velocity of K_V7.2 anterograde vesicles, there was a 45% increase in fluorescence intensity in IM-treated axons (Fig. 3 *C–E*, *Right*).

In contrast, the retrograde trafficking of Na_V1.7 and K_V7.2 containing vesicles was not significantly regulated by IM treatment, both displaying similar flux, intensity, and velocity between IM-treated and control axons (Fig. 3 *F–I*). Together, these results suggest that inflammatory mediators induce a preferential increase in anterograde trafficking of Na_V1.7 over K_V7.2, without a parallel or opposite change in retrograde trafficking.

Inflammatory Mediators Increase the Rate of Insertion of Na_V1.7, but Not K_V7.2, at Distal Axonal Ends, and Do Not Regulate the Removal of Either. We next developed a method to visualize the processes of channel insertion in, and removal from, axonal membranes. DRG neurons were transfected with Halo-tagged channels and cultured in MFCs. Channels at the surface of axons were first labeled using cell-impermeable, red JF549i-Halo-tag ligand and unbound ligand was removed. Then, cell-impermeable, far-red JF635i-Halo-tag ligand was added to the cell media and axons were imaged over the course of 6 h (Fig. 4*A*). Channels which were present at the start of the experiment and labeled with the primary Halo-tag Ligand were removed over time (Fig. 4*B*). In contrast, channels which were inside the axoplasm during the first labeling step and subsequently inserted into the axonal membrane were labeled by the secondary Halo-tag ligand as they were inserted (Fig. 4*C*). The rate of removal of Na_V1.7 channels from the axonal membrane was similar between control and IM-treated axons (Fig. 4*D*). Although there was a statistically significant difference between control and IM-treated axons after 1 h, the effect size was small and is not present at other time points, suggesting that this difference may not be biologically important. The rate of insertion of Na_V1.7 was greater in IM-treated axons, with 51% and 69% increases relative to control at the 5- and 6-h time points, respectively (Fig. 4*E*). In similar experiments completed with K_V7.2, there was no difference in the rate of channel removal (Fig. 4*F* and *H*). While there was a trend toward a reduction of K_V7.2 insertion at some timepoints, these differences were not statistically significant (Fig. 4 *G* and *I*). These results demonstrate a selective increase in the insertion of Na_V1.7 in distal axonal membranes over K_V7.2 in response to inflammatory mediators.

Inflammatory Mediators Increase the Loading of Na_V1.7 into Vesicular Transport Vesicles over K_V7.2. The IM-induced increase in Na_V1.7 anterograde trafficking relative to K_V7.2 could be explained by at least two potential mechanisms: increased loading of Na_V1.7 channels into a similar number of transport vesicles, increased transport of a population of vesicles which preferentially contain Na_V1.7, or a combination of both. To determine which mechanisms underlie this effect, we transfected DRG neurons with both SNAP-Na_V1.7 (SNAP-tag is a self-labeling enzymatic tag which works similarly to Halo-tag, but has a different cognate ligand) and K_V7.2-Halo and performed simultaneous two-color OPAL imaging with and without IM treatment. In neurons which expressed both tagged proteins, we observed frequent cotrafficking of Na_V1.7 and K_V7.2 (Fig. 5*A*), similar to our previous reports (24). The distribution of vesicle intensities was roughly bimodal, with a trough around 100 A.U., allowing vesicles to be classified

as positive for either protein or both (*SI Appendix*, Fig. S3). We observed a significant increase in the proportion of vesicles containing Na_V1.7 in IM-treated axons: the proportion containing only Na_V1.7 increased from 5 to 18% and the proportion containing both Na_V1.7 and K_V7.2 increased from 56 to 69% with IM treatment, while the proportion containing only K_V7.2 decreased from 39 to 13% (Fig. 5 *B* and *C*). We further analyzed the fluorescence intensity of vesicles which contained both channels and found that the relative amount of Na_V1.7 compared to K_V7.2 in each double-positive vesicle increased in response to IM treatment (Fig. 5*D*). Together, these results demonstrate that inflammatory mediators selectively up-regulate both the loading of Na_V1.7 channels into additional transport vesicles and the loading of additional Na_V1.7 in each vesicle.

Discussion

Our results show that inflammatory mediators induce a Na_V1.7-dependent increase in nociceptor activity and upregulation of Na_V1.7 current and surface expression. We determine that the mechanism for this effect is an upregulation of vesicular loading, anterograde trafficking, and insertion of Na_V1.7 into distal axonal membranes without a compensatory change in retrograde trafficking. Importantly, these effects are specific, since similar changes to the current, surface expression, and trafficking of K_V7.2 did not occur (Fig. 6).

These studies begin to clarify several fundamental uncertainties: whether ion channel trafficking contributes to inflammatory pain, which cellular trafficking mechanisms are modulated by inflammation, and whether the trafficking of particular proteins is regulated specifically. To answer these questions, we continue to build upon our recent methodological advances in live-neuron imaging to directly interrogate bidirectional axonal transport, exocytosis, and endocytosis of specific ion channels, as well as activity in distal axons. These abilities allowed us to demonstrate that inflammatory mediators acting on DRG neurons rapidly and specifically up-regulate the anterograde trafficking of Na_V1.7 and cause an increase in axonal activity which is dependent on Na_V1.7 function. Together, these findings implicate the trafficking of Na_V1.7 as a mechanism for inflammatory pain and potential therapeutic target.

Neuronal excitability is a function of the balance of currents produced by the ensemble of channels at the cell surface, which is itself partly a function of the trafficking of channels to and from the surface. The steady-state abundance of a given channel at the distal axon surface is increased by inflows—transcription, translation, anterograde trafficking, and membrane insertion—and decreased by outflows—endocytosis, retrograde trafficking, and degradation. Therefore, the observed increase in Na_V1.7 at the surface of distal axons could conceivably have been due to an upregulation of inflows, downregulation of outflows, or a combination of both. Here, we identify increases in vesicular loading, anterograde trafficking, and insertion in the plasma membrane as the responsible mechanisms for the phenotype and suggest against a role for changes in transcription of Na_V1.7 for this effect. Still, several studies have demonstrated changes in Na_V1.7 expression in response to inflammatory insults *in vivo* over longer time periods, which may further augment increases in trafficking (11, 12, 14, 28). Additionally, other well-demonstrated mechanisms, such as alterations in gating properties of individual channels through posttranslational modifications (29, 30), undoubtedly contribute to increased nociceptor excitability in inflammation. Due to the lack of existing tools to specifically interfere with Na_V1.7 trafficking,

we are unable to determine what portion of the IM-induced increase in axonal excitability is due to the observed changes in channel trafficking versus conductance of individual channels at the membrane. Tools for selective control of the trafficking

of specific proteins might be used in future studies to disentangle these effects (31).

Since neuronal excitability is a function of depolarizing and hyperpolarizing currents through the ensemble of ion channels

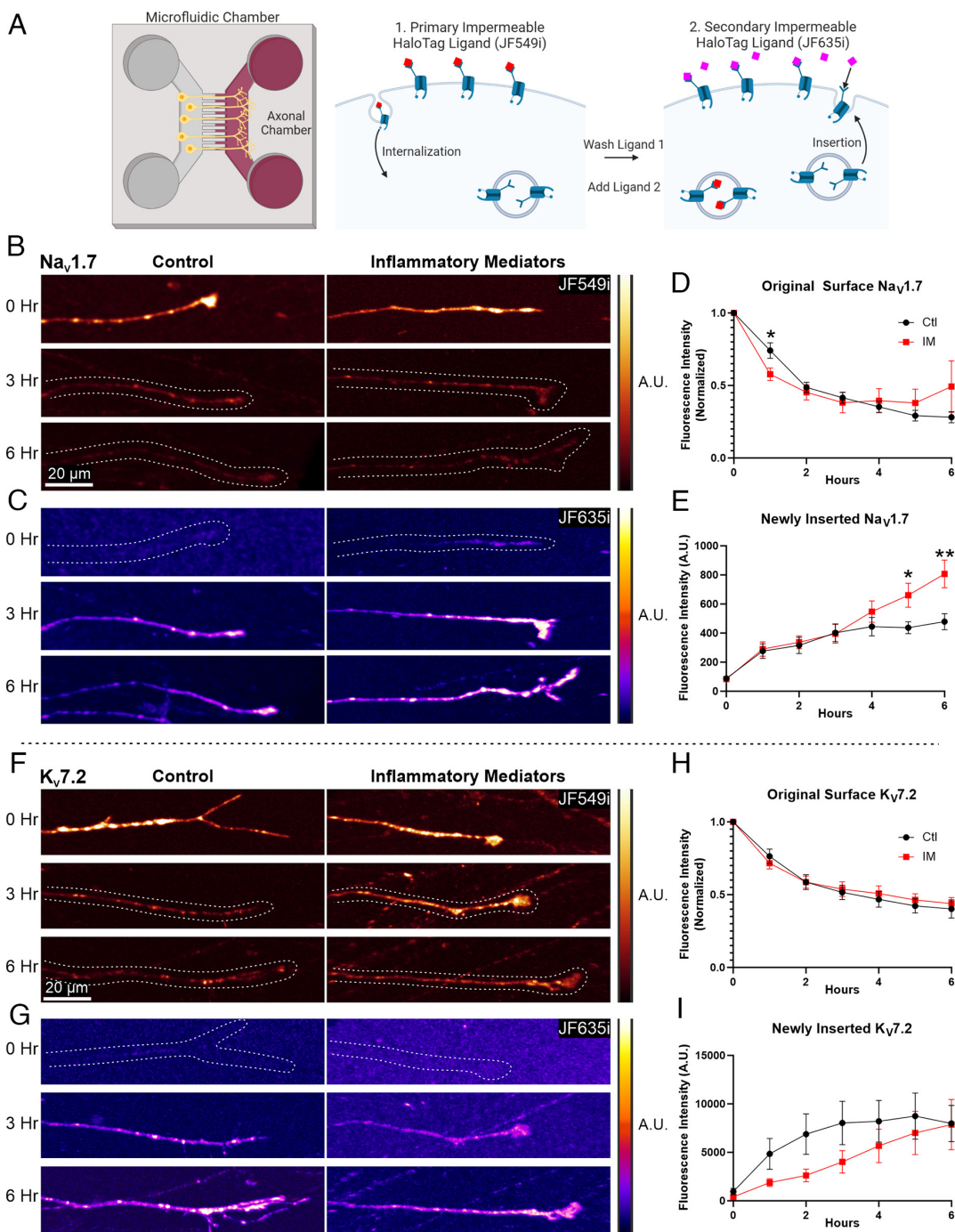


Fig. 4. Inflammatory mediators increase the rate of axonal insertion of $\text{Na}_v1.7$, but not $\text{K}_v7.2$, and do not regulate the removal of either. (A) DRG neurons expressing Halo-tagged channels in MFCs were labeled using this protocol. First, channels at the surface of axons were labeled with cell-impermeable, red JF549i-Halo-tag ligand and excess ligand was thoroughly washed away. Second, axons were exposed to cell-impermeable, far-red JF635i-Halo-tag ligand and imaged using red and far-red imaging for 6 h in the presence of either IM cocktail or normal media (Ctl). Still images from time-lapse movies show that channels present at the cell membrane at the start of the experiment were labeled with JF549i and removed over time (B and F), while channels inserted in the membrane over the course of the experiment were labeled with JF635i over time (C and G). Note that JF635i-Halo-tag ligand fluorescence is lower in its unbound state and increases upon binding to Halo-tag, and thus can remain in the imaging solution without causing significant background fluorescence. Note also that the change in the shape and position of axons over time is due to continued growth. (D) The rate of removal of $\text{Na}_v1.7$ channels originally at the axonal surface is similar between Ctl and IM-treated axons, with a modest but statistically significant difference at the 1-h timepoint ($N = 19$ to 23 axons each). (E) More $\text{Na}_v1.7$ channels are inserted in the membrane of axons treated with IM relative to Ctl, with significant differences at the 5- and 6-h timepoints (51% and 69% increase, respectively) ($N = 30$ to 31 axons each). * $P < 0.05$, ** $P < 0.01$, Mann-Whitney U test. (H) The rate of removal of $\text{K}_v7.2$ channels originally at the axonal surface is similar between Ctl and IM-treated axons ($N = 21$ axons each). (I) Though there is a trend toward less $\text{K}_v7.2$ inserted at the 2-h timepoint, differences did not reach statistical significance at any timepoint. ($N = 21$ axons each).

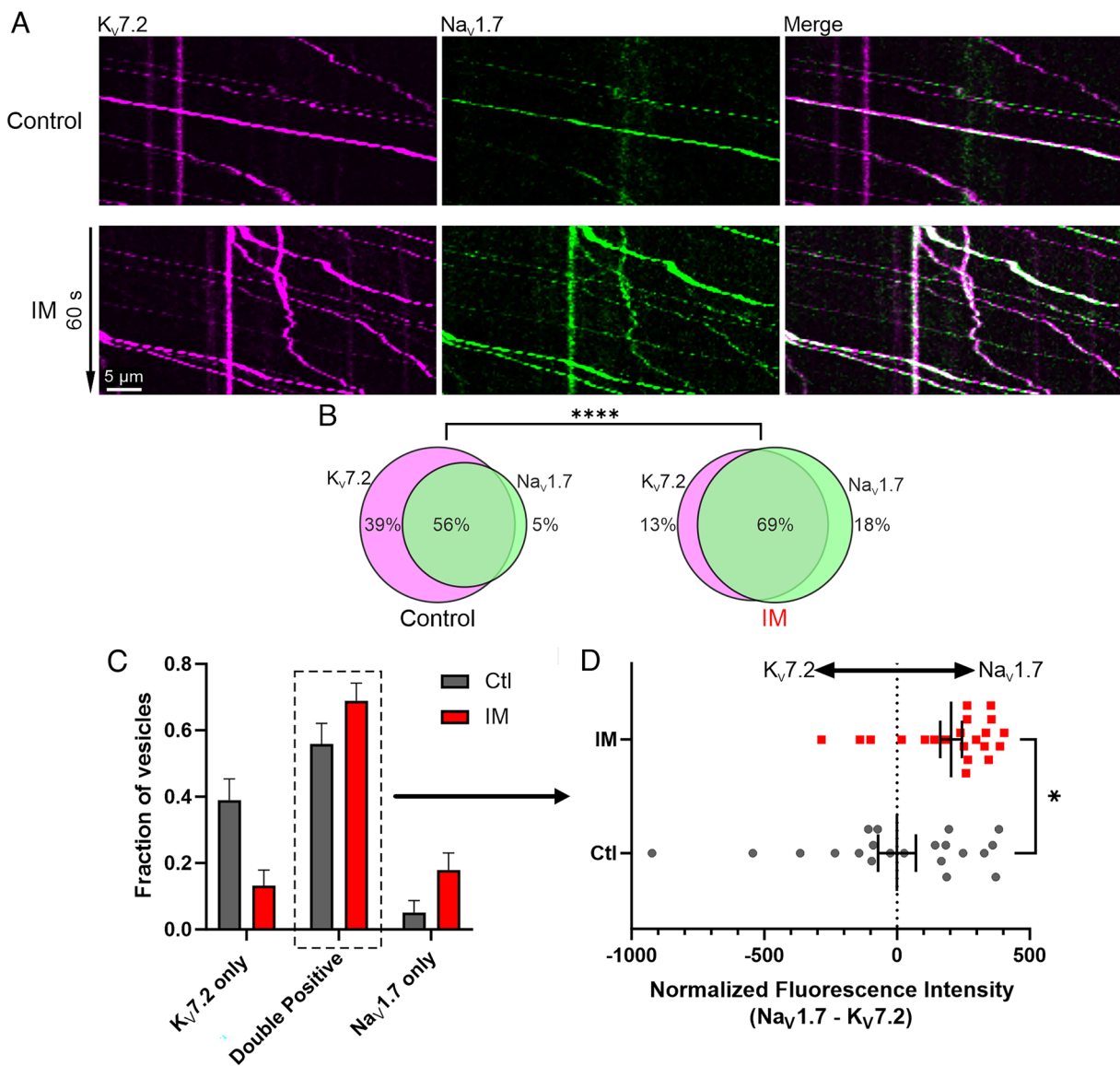


Fig. 5. Inflammatory mediators increase both the proportion of Na_v1.7-carrying vesicles and the relative abundance of Na_v1.7 versus K_v7.2 channels per vesicle. (A) DRG neurons were transfected with SNAP-Na_v1.7 and K_v7.2-Halo and cultured in MFCs for 5 to 6 d. Both soma and axon chambers were then treated for 4 h with either an inflammatory mediator cocktail (IM) or normal media (Ctl). Channels in the soma compartment were labeled with cell-permeable, red JF552-cpSNAP-tag ligand and cell-permeable, far-red JF646-Halo-tag ligand. After labeling, anterograde vesicles carrying both tagged proteins were visualized in the axonal compartment using dual-color red and far-red imaging. Kymographs show vesicles moving along axons, most of which contain both Na_v1.7 and K_v7.2, while a minority only contain one of the proteins. (B and C) Under control conditions, 56% of vesicles contained both channels and 5% contained Na_v1.7 only. After inflammatory treatment, the proportion of vesicles containing Na_v1.7 increased significantly, with 69% containing both channels and 18% containing Na_v1.7 only (Chi-square, $P < 0.0001$, error bars indicate 95% CIs calculated by the Wilson-Brown method). (D) Within vesicles which contained both channels, the relative abundance of Na_v1.7 compared to K_v7.2 was higher in axons which had been treated with IM ($N = 21$ axons each, $P = 0.02$, Mann-Whitney test).

present at the membrane, an increase in depolarizing current could potentially be offset by a proportional increase in hyperpolarizing current. We chose to compare Na_v1.7 and K_v7.2, as they exemplify the classes of depolarizing and hyperpolarizing channels, respectively, and each have demonstrated importance in normal physiology and pain signaling. After inflammatory mediator treatment, we observed consistent increases in Na_v1.7 current, surface expression, anterograde vesicle flux, channels per vesicle, and insertion at the membrane. In contrast, we observed either no difference or a trend toward decrease in these processes for K_v7.2, with the exception of an increase in channels per anterograde vesicle, which was smaller than the corresponding increase for Na_v1.7. Together with our demonstration that IM increases the relative abundance of Na_v1.7 versus K_v7.2 in the same vesicles, these results indicate a potential net increase in depolarizing current. This change would be predicted to cause an increase in excitability, which is further

supported by our finding that inflammation induces an increase in axonal activity which is dependent on Na_v1.7. It is notable that specific inhibition of Na_v1.7 reverses the IM-induced increase in activity but does not eliminate activity in untreated axons. While this indicates that Na_v1.7 current is necessary for IM-induced increase in axonal excitability, it also suggests that some activity can continue under blockade of Na_v1.7 current, which could have potential therapeutic benefits. While other studies have demonstrated that inflammation also increases axonal current and excitability through changes to other ion channels including Na_v1.8, Na_v1.9, and several other types of channels (32–35), our data suggest that increased Na_v1.7 function plays a necessary role.

Some of these results were somewhat unexpected. First, we observed a 45% increase in K_v7.2 anterograde vesicle fluorescence intensity without increases in vesicular flux, vesicular velocity, surface expression, or membrane insertion. This suggests that

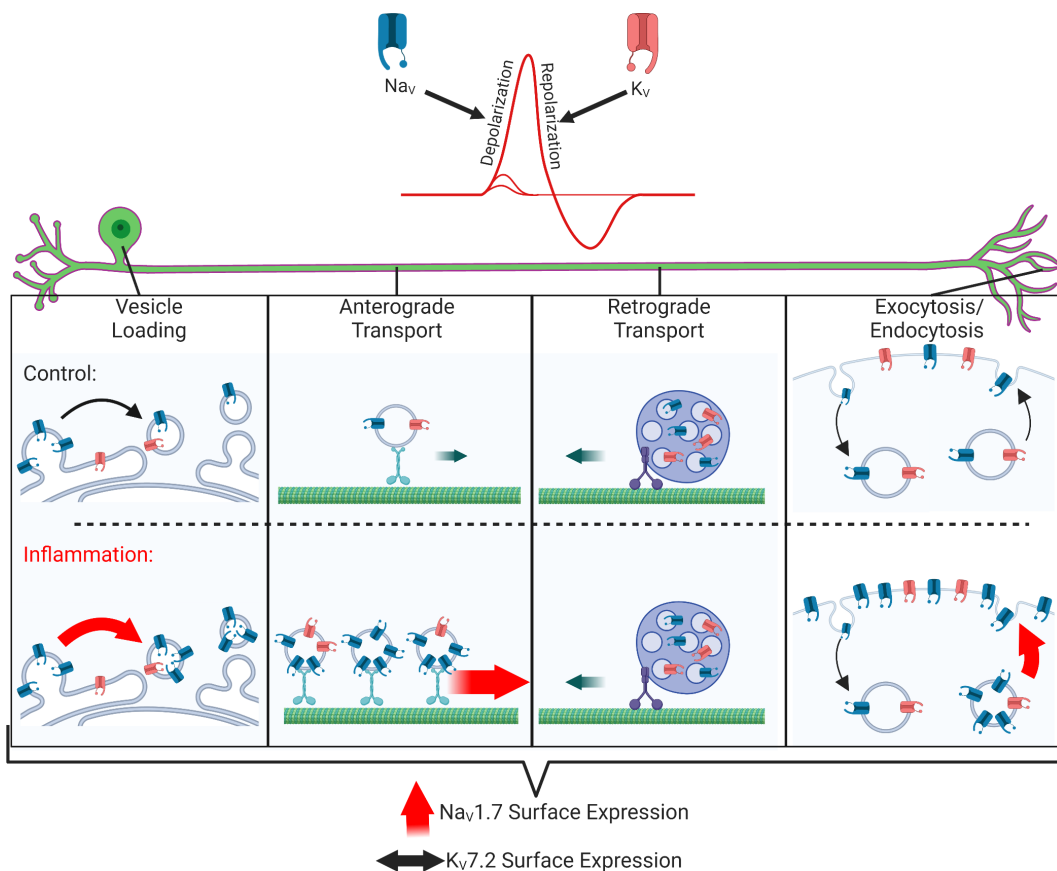


Fig. 6. Inflammatory mediators selectively increase $\text{Na}_v1.7$ surface expression through upregulation of anterograde trafficking and membrane insertion. Schematic of a model mechanism whereby inflammatory mediators selectively increase $\text{Na}_v1.7$ surface expression in axons by increasing anterograde trafficking and insertion in distal axonal membranes without corresponding changes in endocytosis or retrograde trafficking and without similar effects on the trafficking of $\text{K}_v7.2$. The selective upregulation of surface expression by modulation of trafficking of depolarizing $\text{Na}_v1.7$, and not hyperpolarizing $\text{K}_v7.2$, may shift membrane excitability and lead to increased nociceptor activity and pain in inflammation.

while IM has a differential effect on the trafficking of $\text{Na}_v1.7$, there may also be a smaller effect on $\text{K}_v7.2$. However, given that possible signaling pathways downstream of IM (including increased levels of cyclic adenosine monophosphate (cAMP) and activation of protein kinase A (PKA)) are known to have pleiotropic effects on axonal trafficking, multiple effects are not unexpected (36). Further, the fact that the increase in $\text{K}_v7.2$ vesicle brightness does not lead to increased $\text{K}_v7.2$ membrane insertion suggests that there may be multiple mechanisms which separately regulate the distinct processes of axonal trafficking and insertion at the membrane. Last, while these data confirm our previous findings that IM induces upregulation of $\text{Na}_v1.7$ surface expression, the number of anterograde transport vesicles, and the number of channels per vesicle, for reasons that are unclear, we did not observe an increase in vesicle velocity as previously reported (22).

While this study provides detailed information regarding cell biological mechanisms, there are multiple limitations to consider. First, our studies rely on overexpression of exogenous tagged ion channels, which could potentially be trafficked differently than native proteins. However, this does not invalidate the observed differences in the behavior of exogenous channels in IM-treated and control neurons, and we have demonstrated that overexpression does not cause proteins to be trafficked indiscriminately (22, 24). Second, while our reductionist *in vitro* preparation provides mechanistic insight by allowing us to visualize channel trafficking at the level of individual channel proteins, it lacks many components involved in inflammatory pain including glial and immune cells. While our cocktail of inflammatory mediators includes five

important factors, it is certain that the “inflammatory soup” *in vivo* contains other factors which influence neuronal physiology (37). Future studies could explore the effects of individual mediators or recapitulate aspects of *in vivo* interactions by observing ion channel trafficking in the presence of glial or immune cells.

Pain is one of the world’s leading causes of suffering and disability (38). Current treatments are often ineffective and cause serious side effects, including addiction (39, 40). Due to its preferential expression in peripheral pain-sensing neurons and genetically validated role in human pain, $\text{Na}_v1.7$ is a promising target for nonaddictive pain treatment (7, 8). So far, attempts to target $\text{Na}_v1.7$ have taken the strategy of reducing current through channels inserted at the cell membrane (21). However, another strategy to achieve a similar effect is to modulate transport of channels to the cell surface. Implementing this therapeutic strategy requires identifying mechanisms that mediate or modulate the trafficking of specific sodium channels. The present studies demonstrate that the trafficking of $\text{Na}_v1.7$ is regulated specifically in ways that may promote pain. In particular, we show that inflammatory stimuli induce a rapid and specific increase in vesicular loading of $\text{Na}_v1.7$ —a process which could potentially be targeted therapeutically.

Materials and Methods

DNA Constructs. The Halo- $\text{Na}_v1.7$ construct was described previously (22, 24). The engineering of the construct used here was the same as in our previous studies, except that here we used a codon-optimized $\text{Na}_v1.7$ backbone instead of the native sequence. Briefly, human $\text{Na}_v1.7$ was rendered tetrodotoxin resistant

(TTX-R) with the mutation Y362S (41), and the following components were added, in order from the N terminus: 1 to 30 a.a. β 4 signal peptide, 3X myc tag (EQKLI β EDL), Halo-tag enzyme (297 a.a.) (Promega, Madison, WI), 3X HA tag (YPYDVPDYA), 21 a.a. transmembrane segment (β 4 163–183), and 7 a.a. linker (SGLRSAT). SNAP- Na_v 1.7 was constructed similarly, with TTX-R, codon-optimized human- Na_v 1.7, but with the 182 a.a. SNAP_f (New England BioLabs, Ipswich, MA) in place of Halo-tag. K_v7.2-Halo was synthesized by GenScript (Piscataway, NJ), with Halo-tag inserted in an extracellular loop between amino acids 117 and 118, flanked by a three amino acid spacer (GlyAlaGly) (24). Axon-jGCaMP8m was a gift from Marianne Fyhn (Addgene #172719).

Primary Dorsal Root Ganglion (DRG) Neuron Culture and Transfection.

Animal studies followed a protocol approved by the Veterans Administration Connecticut Healthcare System Institutional Animal Care and Use Committee.

DRG neurons were isolated from 2- to 4-d-old Sprague-Dawley rats and transfected as described previously (22, 42). See *SI Appendix* for complete details. Briefly, DRGs were dissected and dissociated, and large debris was filtered. Plasmid DNA was then transfected by electroporation. The DRGs were then carefully seeded onto the somatic chamber of microfluidic chambers (MFCs) and maintained at 37 °C in a 95% air/5% CO₂ (v/v) incubator before use.

Microfluidic Chambers. As described previously (22, 24), MFCs (DOC450, two-chamber 450- μm groove, Xona Microfluidics, Temecula, CA) were bound to glass-bottomed dishes according to manufacturer's instructions. Briefly, MFCs were soaked in ethanol for 1 min, and then air dried before being placed on 50-mm glass-bottomed dishes (P50G-1.55-30-F, MatTek) that were coated with poly-L-lysine (0.5 mg/mL) overnight at 37 °C. The glass surface was washed twice with sterile double-distilled water and then air dried in a sterile hood. The dishes were then coated with laminin (10 $\mu\text{g}/\text{mL}$) for at least 2 h at 37 °C, excess laminin was aspirated, and the dishes were air dried under the hood before MFCs were adhered. Transfected DRG neuron suspension was applied in the soma chamber containing DRG medium with growth factors (50 ng/mg) [nerve growth factor (NGF) and glial cell line-derived neurotrophic factor (GDNF) from PeproTech], and 2 \times growth factors (100 ng/mg) were added to the axonal chamber. Medium was changed to serum-free medium in both chambers after 24 h (Neurobasal medium supplemented with 2% B27, 1% penicillin/streptomycin, same 1:2 ratio of NGF, GDNF in soma and axonal chambers), and 1 μM uridine/5-fluoro-2-deoxyuridine was added to inhibit the growth of fibroblasts and glia.

Inflammatory Mediators. The inflammatory mediator (IM) cocktail consisted of bradykinin (final concentrations: 1 μM), PGE-2 (prostaglandin E2, 10 μM), histamine (10 μM), 5-HT (5-hydroxytryptamine/serotonin, 10 μM), and ATP (15 μM) (all from Sigma-Aldrich) (22, 32, 43). The solution was prepared at 100 \times final concentration and frozen in aliquots until use. Treatment was added to both somatic and axonal MFC chambers.

Calcium Imaging. DRG neurons were transfected with Axon-jGCaMP8m and cultured in MFCs for 5 to 6 d. Both the axon and soma compartments were treated with IM or normal media for 4 h. Then, the treatment was removed by thoroughly washing both chambers with DRG neuronal imaging saline (NIS) (136 mM NaCl, 3 mM KCl, 1 mM MgSO₄, 2.5 mM CaCl₂, 0.15 mM NaH₂PO₄, 0.1 mM ascorbic acid, 20 mM HEPES (N-2-hydroxyethylpiperazine-N-2-ethane sulfonic acid), and 8 mM dextrose (pH 7.4) with NaOH (adjusted to 320 mOsm/liter)). Multiple fields of view containing GCaMP-expressing axonal ends were selected and green time-lapse movies were acquired at 10 Hz (see *SI Appendix* for detailed description of the imaging system). Then, DRG NIS containing 10 nM ProTx-II (Tocris) and 0.1% BSA was added to both chambers by fluid exchange over approximately 5 min. After another 5 min of incubation, the same fields of view were imaged again.

GCaMP-expressing axon endings which were clearly separate from other axons were selected for analysis. Calcium time-course data were extracted from the distal-most 30 μm of axons. Regions of interest, six pixels wide, were generated over this final 30 μm of the axon and the average fluorescence intensity within this region was measured at each timepoint. The percent change in fluorescence at each timepoint was calculated relative to a least-squares regression line that had been fit to the entire time course. Calcium events were defined as any instance where the fluorescence intensity increased by > 8% between two consecutive frames.

Voltage-Clamp Recordings. Macroscopic currents were recorded in voltage-clamp mode using an EPC-10 amplifier and the PatchMaster Next program (HEKA Electronik). Series resistance compensation of 80 to 90% was applied to reduce voltage error. Recordings were sampled at 50 kHz through a low-pass Bessel filter of 2.9 kHz. After achieving the whole-cell configuration, a 5-min delay was applied to allow adequate time for the pipette solution and cytoplasmic milieu to equilibrate. Current density was measured by normalizing peak currents with cell capacitance. Recordings from cells in the IM treatment condition were acquired after 4 h of incubation with the previously described IM cocktail.

N_av1.7. DRGs from adult (4 to 6 wk old) Na_v 1.8-KO mice were harvested and dissociated as described previously (42). After trituration, neurons were transfected with 2.0 μg eGFP-2A-h Na_v 1.7 (with the Y362S substitution to render the channel TTX resistant) using a Nucleofector IIS (Lonza) and Amaxa Basic Neuron small cell number (SCN) Nucleofector Kit. Cells were plated into 24-well plates containing coverslips coated with poly-L-lysine and laminin and maintained in DRG media at 37 °C for 24 h after transfection before acquiring patch-clamp recordings.

To measure Na_v 1.7 currents, small-diameter (<25 μM) DRG neurons with green fluorescence were selected for whole-cell voltage-clamp recording. Patch pipettes were fabricated from borosilicate glass (World Precision Instruments) using a P-97 puller (Sutter Instruments) and fire-polished for a resistance of 0.8 to 1.2 megaohms when filled with internal solution. The pipette internal solution contained (in mM): 140 CsF, 10 NaCl, 1.1 EGTA (Ethyleneglycol- bis- β -aminoethyl)-N,N,N',N'-tetraacetic Acid), 10 HEPES, and 20 dextrose (pH 7.3 with CsOH, adjusted to 310 mOsm/L with dextrose). External bath solution contained (in mM): 140 NaCl, 20 TEA-Cl, 3 KCl, 1 CaCl₂, 1 MgCl₂, 10 HEPES, 5 sucrose, 0.1 CdCl₂, and 0.001 TTX (pH 7.3 with NaOH, adjusted to 320 mOsm/L with sucrose). Currents were evoked by 100 ms depolarizing voltage steps from -80 to +40 mV in 5-mV increments from a holding potential of -100 mV.

K_v7 (M-Current). Neonatal rat DRG neurons were harvested and dissociated as described previously (42) and plated onto 24-well plates containing coverslips coated with poly-L-lysine and laminin and maintained in DRG media for 2 h before acquiring patch-clamp recordings.

To measure endogenous M-currents, small-diameter (<25 μM) DRG neurons were selected for whole-cell voltage-clamp recording. Patch pipettes were fabricated from borosilicate glass (World Precision Instruments) using a P-97 puller (Sutter Instruments) and fire-polished for a resistance of 4.0 to 5.0 M Ω when filled with internal solution. The pipette internal solution contained (in mM): 80 K-acetate, 30 KCl, 1 CaCl₂, 3 EGTA, 40 HEPES, and 3 MgCl₂ (pH 7.3 w/ KOH, adjusted to 310 mOsm/L with dextrose). External bath solution contained (in mM): 144 NaCl, 2.5 KCl, 2 CaCl₂, 0.5 MgCl₂, 5 HEPES, 10 dextrose, 0.001 TTX, 0.1 CdCl₂, and 0.02 ZD-7288 (pH 7.3 w/ NaOH, adjusted to 320 mOsm/L with dextrose). TTX, CdCl₂, and ZD-7288 were included in the bath to block voltage-gated Na⁺, voltage-gated Ca²⁺, and HCN channels, respectively.

A standard voltage protocol was applied to evoke M-current (44–46). Cells were held at -20mV. A series of 500 ms hyperpolarizing pulses from -20 to -100 mV were applied in 5 mV increments. M-currents were determined using the methods described by Tzour et al. (46). Briefly, voltage steps induced slow current relaxations which represent slow M-current deactivation. Current relaxations were fit by exponential curves (beginning after the capacitance artifact) and were extrapolated to the beginning of the command pulse. M-current amplitudes were assessed as the difference between the peak current at command onset and the steady state current at command offset.

RT-qPCR. DRG neurons were isolated as described above and plated into 6-well cell culture plates (Corning) which had been precoated with poly-D-lysine for 1 h at 37 °C and subsequently with laminin for 2 h at 37 °C. The cells were then treated with IM cocktail for 4 or 24 h. After the cells had been in culture for 48 h, RNA was extracted using the RNeasy® kit (Qiagen) according to the manufacturer's protocol. Complementary DNA was generated from 100 ng of DRG RNA using Bio-Rad iScript™ Reverse Transcription Supermix. The following Prime-PCR probe Bio-Rad assays were used: Actb (qRnoCIP0050804), Gapdh (qRnoCIP0050838), and Na_v 1.7 (qRnoCIP0023430). K_v7.2 RNA was measured using Rat Kcnq2 TaqMan® Gene Expression Assay (Rn00591249_m1, Fisher Scientific). 10 μL PCR reactions were run with Bio-Rad SsoAdvanced™ Universal Probes Supermix in technical triplicate for each sample using the Bio-Rad CFX96 Touch System with the following thermal cycling procedure; 95 °C for 30 s followed by 40 cycles of 95 °C

for 10 s and 60 °C for 20 s. Three independent cultures (biological replicates) were used for each condition and three technical replicates were averaged for each biological replicate. The target genes were normalized to Actin and Gapdh expression. No reverse transcriptase controls and no template controls were used for each condition, and if any control reaction passed threshold with a C_q less than 35, data from that sample were excluded. The relative quantity and normalized expression data ($\Delta\Delta C_q$) were processed using Bio-Rad CFX Maestro.

Channel Trafficking Assays. These studies include variations on the Optical Pulse-chase Axonal Long-distance (OPAL) imaging method described previously (22, 24). DRG neurons were transfected with Halo- and/or SNAP-tagged constructs and cultured in MFCs for 5 to 7 d. For experiments using Halo-tag only, 100 nM Janelia Fluor (JF) Halo-tag ligand was added to one chamber or both chambers for 15 min and then thoroughly washed. All Halo-tag ligand- and SNAP-tag ligand-conjugated Janelia Fluor labels (47, 48) were generous gifts of L. D. Lavis and J. B. Grimm (Janelia Research Campus).

All live-cell experiments were performed at 37 °C using a stage incubator (Tokai Hit, Shizuoka, Japan). For experiments with imaging durations of 1 h or less (all but the channel insertion and removal assay), neurons were labeled and imaged in DRG NIS. For the channel insertion and removal assay, neurons were labeled and imaged in serum-free medium without phenol red and in the presence of 5% CO₂ atmosphere.

Anterograde and Retrograde Trafficking. DRG neurons were transfected with Halo-Na_v1.7 or K_v7.2-Halo and cultured in MFCs for 5 d. Both soma and axon chambers were then treated for 4 h with either IM or Ctl. Channels in the soma compartment were labeled with cell-permeable, red JF549-Halo-tag ligand, while channels in the axonal compartment were labeled with cell-permeable, far-red JF646-Halo-tag ligand. After labeling, anterograde vesicles were visualized using red imaging and separately, retrograde vesicles were visualized using far-red imaging as they were transported between the two chambers.

Resulting movies were opened in ImageJ, and the KymographClear toolset was used to create kymographs of the selected axons (49). Specifically, axons containing trafficked vesicles were traced manually using a segmented line, and KymographClear extracted the signal under that line and converted it into a two-dimensional image with distance along the axon on the x axis and time on the y axis. Two kymographs were generated for each axon: one from the red movie showing anterograde trafficking and one from the far-red movie showing retrograde trafficking. Kymographs were analyzed using the automated kymograph analysis software KymoButler (50), which uses a machine learning algorithm to trace vesicle tracks. Vesicle flux was determined by counting the number of vesicles which crossed the midline of the kymograph in either the anterograde or retrograde direction. Vesicle intensity was determined as the average of fluorescence values of pixels along the vesicle track, minus the background signal of the kymograph (defined as the modal value for that kymograph). Vesicle velocity was calculated as the average over the duration of the track, including pauses and stops. The fluorescence intensities and velocities of multiple vesicles within an axon were averaged. Only axons that were separate from other axons were analyzed.

Channel Surface Labeling and Endocytosis. DRG neurons were transfected with Halo-Na_v1.7 or K_v7.2-Halo and cultured in MFCs for 5 d. Both soma and axon chambers were then treated for 4 h with either IM or Ctl. Axonal surface channels were then labeled with cell-impermeable JF635i-Halo-tag ligand (48) and unbound ligand was washed away. After labeling, the dishes were placed in a stage-top incubator and multiple axons (in ~3 fields of view) were imaged every ~4 s over the course of an hour. Na_v1.7 surface expression was quantified as the average fluorescence intensity of the most distal 30 μm of labeled axons in the first frame of the movie, before significant endocytosis has occurred. Because these movies were acquired at a lower frame rate (~0.25 Hz), vesicle tracks along kymographs were discontinuous, which interfered with automated analysis. Thus, kymographs were generated as above, but endosome tracks were traced and analyzed manually: fluorescence intensity of each endosome was measured and background subtracted; each endosome within a kymograph was counted, and the total was normalized to the length of the movie to calculate endosome flux per 60 min; velocity (instantaneous, excluding stops) was extracted using KymographDirect (49).

Channel Insertion and Removal. DRG neurons were transfected with Halo-Na_v1.7 or K_v7.2-Halo and cultured in MFCs for 5 d. Na_v1.7 channels at the surface of axons were labeled with cell-impermeable, red JF549i-Halo-tag ligand (100

nM) for 15 min and excess ligand was thoroughly washed away. Then, axons were exposed to cell-impermeable, far-red JF635i-Halo-tag ligand (10 nM), which was maintained throughout the experiment. JF635i-Halo-tag ligand was used at a lower concentration (10 instead of 100 nM) to minimize fluorescent background while still allowing for rapid labeling of newly inserted proteins. Labeled axons were identified and imaged using red and far-red imaging in a stage-top incubator for 6 h in serum-free media with or without IM cocktail. For each time point and field of view, confocal z-stacks were acquired in both red and far-red imaging channels. For analysis, z-stacks were processed by maximum-intensity projection and the mean fluorescence intensity of each color was measured within the distal-most 30 μm of the axon. The background of the maximum intensity projection (modal intensity value) was determined for each color, timepoint, and field of view and was subtracted from each intensity measurement. Original surface Na_v1.7 (JF549i) signal was normalized to the value at time 0 for each axon.

Cotrafficking. DRG neurons were transfected with SNAP-Na_v1.7 and K_v7.2-Halo and cultured in MFCs for 5 to 6 d. Both soma and axon chambers were then treated for 4 h with either an inflammatory mediator cocktail (IM) or normal media (Ctl). JF646-Halo-tag ligand and JF552-cpSNAP-tag ligand (100 nM each) were added to the soma chamber for 30 min before imaging. Axons within the axonal chamber were then imaged in red and far-red by rapid laser and color filter switching. Axons were selected for analysis if there was at least one moving vesicle containing each protein visible in the axon, indicating that the neuron had been transfected with both constructs. Kymographs of these axons were created, and the fluorescence intensity in both colors was measured for each vesicle manually. The background was measured for each color and kymograph, and subtracted from the vesicle measurements. A cutoff of 100 A.U. was used to categorize vesicles as positive or negative for each protein. To compare the amount of Na_v and K_v channels in individual double-positive vesicles, the K_v7.2 fluorescence intensity was subtracted from the Na_v1.7 intensity. The values for all of the vesicles within a given axon were averaged. The distributions were then normalized to the control condition by subtracting the mean of the control from each data point.

Image and Statistical Analyses. The experimenter was blind to the treatment condition during data acquisition and analysis. Images were processed using either ImageJ or Imaris. Images which are intended to be compared to each other were processed identically and displayed with the same maximum, minimum, and gamma values. Statistical analysis was performed and graphs were formatted using GraphPad Prism. Summary data are shown as mean ± SEM. Because the characteristics of multiple vesicles within a given axon may be correlated with each other, the measurements of fluorescence intensity and velocity for vesicles within each axon were averaged and the resulting axon averages were treated as statistically independent measurements. Distributions were first tested for normality using the Kolmogorov-Smirnov test. If each group being compared followed normality, they were compared using unpaired two-tailed Student's *t* test. If not, they were compared using the two-tailed Mann-Whitney test. Multiple-group comparisons were made using ANOVA with Dunn's multiple comparisons test. For the calcium imaging experiment, there were both paired and unpaired comparisons, and the data were not normally distributed. Thus, paired comparisons were made with the Wilcoxon test and unpaired comparisons were made with the Mann-Whitney test, and all *P* values were subject to Bonferroni correction (*N* = 3). Comparisons of proportions were made by the Chi-square test. Significance was set at *P* < 0.05. Each experiment was repeated with at least three independent samples. Schematics were created with BioRender.com.

Data, Materials, and Software Availability. Research Dataset data have been deposited in Dryad (<https://doi.org/10.5061/dryad.hx3ffb gjg>) (51).

ACKNOWLEDGMENTS. We thank Elizabeth J. Akin, Shawn Ferguson, David Zenisek, Emile Boulpaep, Angeliki Louvi, Fred Gorelick, and Reiko Fitzsimonds for helpful discussions. We thank Luke Lavis and Jonathan Grimm for the Janelia Fluors and helpful discussions. This work was supported in part by Merit Review Award B9253-C and BX004899 from the U.S. Dept. of Veterans Affairs Rehabilitation Research and Development Service and Biomedical Laboratory Research and Development Service, respectively (S.G.W. and S.D.D.-H.), and by grant 2R01-NS-021501 from the National Institute of Neurological Disorders and Health, and by grants from

the Paralyzed Veterans of America, the Taylor Foundation, and The Erythromelalgia Association. The Center for Neuroscience & Regeneration Research is a Collaboration of the Paralyzed Veterans of America with Yale University. G.P.H-R. is supported by National Institute of Neurological Disorders and Stroke 1F31NS122417-01. G.P.H-R. and S.T. are supported by NIH/National Institute of General Medical Sciences Medical Scientist Training Program T32GM007205.

Author affiliations: ^aMedical Scientist Training Program, Yale University School of Medicine, New Haven, CT 06520; ^bCenter for Neuroscience and Regeneration Research, Yale University School of Medicine, New Haven, CT 06510; ^cDepartment of Neurology, Yale University School of Medicine, New Haven, CT 06510; ^dRehabilitation Research Center, Veterans Affairs Connecticut Healthcare System, West Haven, CT 06516; ^eCellular and Molecular Physiology Graduate Program, Yale University School of Medicine, New Haven, CT 06520; and ^fInterdepartmental Neuroscience Graduate Program, Yale University School of Medicine, New Haven, CT 06520

1. L. Yang *et al.*, Human and mouse trigeminal ganglia cell atlas implicates multiple cell types in migraine. *Neuron* **110**, 1806–1821.e8 (2022).
2. A. I. Basbaum, D. M. Bautista, G. Scherrer, D. Julius, Cellular and molecular mechanisms of pain. *Cell* **139**, 267–284 (2009).
3. J. D. Loeser, R. Melzack, Pain: An overview. *Lancet* **353**, 1607–1609 (1999).
4. S. G. Waxman, G. W. Zamponi, Regulating excitability of peripheral afferents: Emerging ion channel targets. *Nat. Neurosci.* **17**, 153–163 (2014).
5. A. L. Hodgkin, A. F. Huxley, Currents carried by sodium and potassium ions through the membrane of the giant axon of Loligo. *J. Physiol.* **116**, 449–472 (1952).
6. I. Estadella *et al.*, Endocytosis: A turnover mechanism controlling ion channel function. *Cells* **9**, 1833 (2020).
7. D. L. Bennett, A. J. Clark, J. Huang, S. G. Waxman, S. D. Dib-Hajj, The role of voltage-gated sodium channels in pain signaling. *Physiol. Rev.* **99**, 1079–1151 (2019).
8. S. D. Dib-Hajj, S. G. Waxman, Sodium channels in human pain disorders: Genetics and pharmacogenomics. *Annu. Rev. Neurosci.* **42**, 87–106 (2019).
9. M. A. Mis *et al.*, Resilience to pain: A peripheral component identified using induced pluripotent stem cells and dynamic clamp. *J. Neurosci.* **39**, 382–392 (2019).
10. J.-H. Yuan *et al.*, KCNQ variants and pain modulation: A missense variant in Kv7.3 contributes to pain resilience. *Brain Commun.* **3**, fcab212 (2021).
11. J. A. Black, S. Liu, M. Tanaka, T. R. Cummins, S. G. Waxman, Changes in the expression of tetrodotoxin-sensitive sodium channels within dorsal root ganglia neurons in inflammatory pain. *Pain* **108**, 237–247 (2004).
12. H. J. Gould *et al.*, Ibuprofen blocks changes in nav 1.7 and 1.8 sodium channels associated with complete freund's adjuvant-induced inflammation in rat. *J. Pain* **5**, 270–280 (2004).
13. I. T. Strickland *et al.*, Changes in the expression of NaV1.7, NaV1.8 and NaV1.9 in a distinct population of dorsal root ganglia innervating the rat knee joint in a model of chronic inflammatory joint pain. *Euro. J. Pain* **12**, 564–572 (2008).
14. L. Liang, L. Fan, B. Tao, M. Yaster, Y.-X. Tao, Protein kinase B/Akt is required for complete freund's adjuvant-induced upregulation of Nav1.7 and Nav1.8 in primary sensory neurons. *J. Pain* **14**, 638–647 (2013).
15. Y. Li *et al.*, DRG voltage-gated sodium channel 1.7 is upregulated in paclitaxel-induced neuropathy in rats and in humans with neuropathic pain. *J. Neurosci.* **38**, 1124–1136 (2018).
16. J. E. Linley *et al.*, Inhibition of M current in sensory neurons by exogenous proteases: A signaling pathway mediating inflammatory nociception. *J. Neurosci.* **28**, 11240–11249 (2008).
17. K. Rose *et al.*, Transcriptional repression of the M channel subunit Kv7.2 in chronic nerve injury. *Pain* **152**, 742–754 (2011).
18. J. A. Black, N. Frézel, S. D. Dib-Hajj, S. G. Waxman, Expression of Nav1.7 in DRG neurons extends from peripheral terminals in the skin to central preterminal branches and terminals in the dorsal horn. *Mol. Pain* **8**, 1744–8069 (2012).
19. C. H. King, S. S. Scherer, Kv7.5 is the primary Kv7 subunit expressed in C-fibers. *J. Comp. Neurol.* **520**, 1940–1950 (2012).
20. A. Abd-Elsayed, M. Jackson, S. L. Gu, K. Fiala, J. Gu, Neuropathic pain and Kv7 voltage-gated potassium channels: The potential role of Kv7 activators in the treatment of neuropathic pain. *Mol. Pain* **15**, 1744806919864256 (2019).
21. M. Alsalam, G. P. Higerd, P. R. Effraim, S. G. Waxman, Status of peripheral sodium channel blockers for non-addictive pain treatment. *Nat. Rev. Neurol.* **16**, 689–705 (2020).
22. E. J. Akin *et al.*, Building sensory axons: Delivery and distribution of NaV1.7 channels and effects of inflammatory mediators. *Sci. Adv.* **5**, eaax4755 (2019).
23. E. J. Akin *et al.*, Paclitaxel increases axonal localization and vesicular trafficking of Nav1.7. *Brain* **144**, 1727–1737 (2021).
24. G. P. Higerd-Rusli *et al.*, Depolarizing NaV and hyperpolarizing KV channels are co-trafficked in sensory neurons. *J. Neurosci.* **42**, 4794–4811 (2022).
25. S. Grodem *et al.*, An updated suite of viral vectors for in vivo calcium imaging using local and retro-orbital injections. bioRxiv [Preprint] (2021). <https://doi.org/10.1101/2021.05.14.443815> (Accessed 8 August 2022).
26. W. A. Schmalhofer *et al.*, ProTx-II, a selective inhibitor of NaV1.7 sodium channels, blocks action potential propagation in nociceptors. *Mol. Pharmacol.* **74**, 1476–1484 (2008).
27. C. Tsantoulas, S. B. McMahon, Opening paths to novel analgesics: The role of potassium channels in chronic pain. *Trends Neurosci.* **37**, 146–158 (2014).
28. R. Y. Bi, Y. Ding, Y. H. Gan, Non-steroidal anti-inflammatory drugs attenuate hyperalgesia and block upregulation of trigeminal ganglionic sodium channel 1.7 after induction of temporomandibular joint inflammation in rats. *Chin. J. Dent. Res.* **19**, 35–42 (2016).
29. S. Stamboulian *et al.*, ERK1/2 mitogen-activated protein kinase phosphorylates sodium channel Nav1.7 and alters its gating properties. *J. Neurosci.* **30**, 1637–1647 (2010).
30. Y. Li *et al.*, Nav1.7 is phosphorylated by Fyn tyrosine kinase which modulates channel expression and gating in a cell type-dependent manner. *Mol. Pain* **14**, 174480691878222 (2018).
31. G. Boncompain *et al.*, Synchronization of secretory protein traffic in populations of cells. *Nat. Methods* **9**, 493–498 (2012).
32. Z.-Y. Tan *et al.*, Tetrodotoxin-resistant sodium channels in sensory neurons generate slow resurgent currents that are enhanced by inflammatory mediators. *J. Neurosci.* **34**, 7190–7197 (2014).
33. F. Amaya *et al.*, The voltage-gated sodium channel Nav1.9 is an effector of peripheral inflammatory pain hypersensitivity. *J. Neurosci.* **26**, 12852–12860 (2006).
34. M. Eisenhut, H. Wallace, Ion channels in inflammation. *Phlügers Arch.* **461**, 401–421 (2011).
35. A. N. Akopian *et al.*, The tetrodotoxin-resistant sodium channel SNS has a specialized function in pain pathways. *Nat. Neurosci.* **2**, 541–548 (1999).
36. M. O'Donnell, R. K. Chance, G. J. Bashaw, Axon growth and guidance: Receptor regulation and signal transduction. *Annu. Rev. Neurosci.* **32**, 383–412 (2009).
37. F. Marchand, M. Peretti, S. B. McMahon, Role of the immune system in chronic pain. *Nat. Rev. Neurosci.* **6**, 521–532 (2005).
38. S. P. Cohen, L. Vase, W. M. Hooten, Chronic pain: An update on burden, best practices, and new advances. *Lancet* **397**, 2082–2097 (2021).
39. A. Baldini, M. Von Korff, E. H. Lin, A review of potential adverse effects of long-term opioid therapy: A practitioner's guide. *Prim. Care Companion CNS disord.* **14**, PCC.11m01326 (2012).
40. C. Staahl, A. E. Olesen, T. Andreassen, L. Arendt-Nielsen, A. M. Drewes, Assessing efficacy of non-opioid analgesics in experimental pain models in healthy volunteers: An updated review. *Br. J. Clin. Pharmacol.* **68**, 322–341 (2009).
41. R. I. Herzog, T. R. Cummins, F. Ghassemi, S. D. Dib-Hajj, S. G. Waxman, Distinct repriming and closed-state inactivation kinetics of Nav1.6 and Nav1.7 sodium channels in mouse spinal sensory neurons. *J. Physiol.* **551**, 741–750 (2003).
42. S. D. Dib-Hajj *et al.*, Transfection of rat or mouse neurons by biolistics or electroporation. *Nat. Protocols* **4**, 1118–1126 (2009).
43. J. R. F. Hockley *et al.*, Multiple roles for NaV1.9 in the activation of visceral afferents by noxious inflammatory, mechanical, and human disease-derived stimuli. *Pain* **155**, 1962–1975 (2014).
44. T. Yu *et al.*, KCNQ2/3/5 channels in dorsal root ganglion neurons can be therapeutic targets of neuropathic pain in diabetic rats. *Mol. Pain* **14**, 1744806918793229 (2018).
45. Q. Zheng *et al.*, Suppression of KCNQ/M (Kv7) potassium channels in dorsal root ganglion neurons contributes to the development of bone cancer pain in a rat model. *Pain* **154**, 434–448 (2013).
46. A. Tzour *et al.*, Kv7/M channels as targets for lipopolysaccharide-induced inflammatory neuronal hyperexcitability. *J. Physiol.* **595**, 713–738 (2017).
47. J. B. Grimm *et al.*, A general method to improve fluorophores for live-cell and single-molecule microscopy. *Nat. Methods* **12**, 244–250 (2015).
48. C. T. H. Jonker *et al.*, Accurate measurement of fast endocytic recycling kinetics in real time. *J. Cell Sci.* **133**, jcs231225 (2020).
49. P. Mangeol, B. Prevo, E. J. Peterman, KymographClear and KymographDirect: Two tools for the automated quantitative analysis of molecular and cellular dynamics using kymographs. *Mol. Biol. Cell* **27**, 1948–1957 (2016).
50. M. A. Jakobs, A. Dimitracopoulos, K. Franze, KymoButler, a deep learning software for automated kymograph analysis. *Elife* **8**, e42288 (2019).
51. G. P. Higerd-Rusli *et al.*, Inflammation differentially controls transport of depolarizing Nav versus hyperpolarizing KV channels to drive rat nociceptor activity. *Dryad*. <https://doi.org/10.5061/dryad.hx3ftfbjg5>. Deposited 8 January 2023.